Distributionally Robust Chance-Constrained Optimal Load Shedding Model for Active Distribution Networks Based on KDE

Xiaotong Qi[*], Wei Liu[†], Hongxi Chen[‡], Bo Yu[§], Li Yang[¶]

April 7, 2026

Abstract

With the high penetration of distributed energy resources in active distribution networks(ADNs), forecast errors from renewables and loads pose significant risks of bilateral violations, including overvoltage/undervoltage and line overloads. To address this challenge, this paper proposes a KDE-DRCCO model that integrates kernel density estimation (KDE) with distributionally robust chance-constrained optimization (DRCCO). Leveraging the radial topology of ADNs, a linearized Distflow model is adopted to establish a linear dependency between decision variables and uncertainties. A data-driven KDE method is employed to capture the forecast error distributions, which enables an exact convex reformulation of the bilateral chance constraints on voltages and line flows using conditional value-at-risk (CVaR) approximation and duality theory. Compared with traditional moment-based ambiguity set approaches, the proposed model significantly reduces the economic loss caused by over-conservatism, achieving a better balance between operational economy and reliability. Simulations on modified IEEE 33-bus and modified IEEE 123-bus systems demonstrate that the proposed model effectively reduces total operating costs while ensuring system security and robustness.

Nomenclature

Symbol	Description
	Sets and Indices
$\mathcal{I}$	Set of nodes, $\mathcal{I} = \{0, 1, \ldots, n\}$, where node 0 denotes the substation
$\mathcal{B}$	Set of branches, $(i, j) \in \mathcal{B}$ denotes the branch from node i to j
$\mathcal{I}_{\mathrm{DG}}$	Set of nodes equipped with distributed generators (DGs)
$\mathcal{T}$	Set of time periods
$\mathcal{S}$	Set of line capacity linearization constraints, $\mathcal{S} = \{1, 2, \ldots, 12\}$
$\mathcal{W}(j)$	Set of node j and all its downstream nodes
	Decision Variables

[*]Dalian University of Technology, China. These authors contributed equally to this work.

[†]Beijing Normal University at Zhuhai, China. These authors contributed equally to this work.

[‡]Dalian University of Technology, China.

[§]Chongqing Normal University, China.

[¶]Corresponding author: yangli96@dlut.edu.cn. Leicester International Institute, Dalian University of Technology, Panjin, Liaoning 124221, China.

Table 1 – Continued

Symbol	Description
$p_{i,t}^{\text{cut}}$	Active load shedding power at node i in time period t
$q_{i,t}^{\text{cut}}$	Reactive load shedding power at node i in time period t
$\lambda_{i,t}$	DG curtailment ratio at node i in time period t, $\lambda_{i,t} \in [0,1]$
p_t^+, p_t^-	Power purchased from and sold to the main grid in time period t
	State Variables
$P_{ij,t}, Q_{ij,t}$	Active and reactive power flow on branch (i,j) in time period t
$V_{i,t}$	Squared voltage magnitude at node i in time period t (except in the exact BFM)
$p_{i,t}, q_{i,t}$	Net active and reactive power demand at node i in time period t
	Parameters
r_{ij}, x_{ij}	Resistance and reactance of branch (i,j)
ℓ_{ij}	Squared current on branch (i,j), $\ell_{ij} = (P_{ij}^2 + Q_{ij}^2)/v_i$
$p_{i,t}^{\text{L}}, q_{i,t}^{\text{L}}$	Forecasted active and reactive load demand at node i in time period t
$p_{i,t}^{\text{DG}}$	Forecasted active DG output at node i in time period t
R_{ij}, X_{ij}	Sum of resistances and reactances on the common path from the root node to nodes i and j
$S_{ij}^{\max}$	Apparent power capacity limit of branch (i,j)
$V_{\min}, V_{\max}$	Lower and upper voltage safety limits
η_1, η_2, η_3	Electricity purchase price, electricity sale price, and load shedding penalty coefficient
Δt	Duration of a single time period
a_s, b_s, c_s	The s-th set of coefficients for line capacity linearization
	Random Variables and Ambiguity Sets
$\tilde{p}_{i,t}^{\text{L}}, \tilde{p}_{i,t}^{\text{DG}}$	Forecast errors of load and DG (random variables)
ξ_t	Random perturbation vector in time period t, $\xi_t \in \mathbb{R}^N$
$\mathcal{D}_t$	Probability distribution ambiguity set in time period t
Λ_ϕ^τ	ϕ-divergence-based weight ambiguity set
τ	Radius of the ambiguity set, controlling the degree of distributional robustness
ϵ	Allowable violation probability of chance constraints
	Auxiliary Symbols
$\overline{\bullet}, \widetilde{\bullet}$	Deterministic forecast value and forecast error of a variable, respectively
$g(\mathbf{x}, \xi)$	Affinely transformed random variable, $g(\mathbf{x}, \xi) = \alpha^\top(\mathbf{x})\xi + \beta(\mathbf{x})$
h	Bandwidth parameter of KDE
$k(\cdot)$	Gaussian kernel function
M	Number of historical samples

1 Introduction

Active distribution networks (ADNs), as an important component of future smart grids, achieve active management and optimal operation of distribution networks by integrating distributed energy resources, energy storage systems, flexible loads, etc. However, the high penetration of distributed energy resources also brings many challenges, such as the intermittency and uncertainty of photovoltaic and wind power, spatial-temporal mismatches between supply and demand, and voltage violations caused by reverse power flows. Traditional distribution network operation models typically assume that loads and distributed energy outputs are deterministic parameters, which struggle to cope with random fluctuations in actual operation [1].

Optimal load shedding (OLS), as an important preventive and corrective control measure, can ensure system security by shedding some non-critical loads when overloading or voltage violations occur. Existing studies are mostly based on deterministic models for optimization [2, 3], ignoring the risks brought by uncertainties. Some studies employ stochastic programming [4] or traditional robust optimization [2] to handle uncertainties. However, the former requires exact probability distribution assumptions and suffers from high computational burdens, while the latter tends to be overly conservative as it protects against all possible scenarios, leading to economic losses.

In recent years, distributionally robust optimization (DRO) has shown superiority in handling uncertainties by constructing ambiguity sets that characterize the uncertainty of probability distributions, optimizing system performance under a certain confidence level [5, 6, 7]. Rayati et al. [5] applied distributionally robust chance-constrained (DRCC) optimization to the day-ahead scheduling of ADNs, constructing ambiguity sets using first- and second-order moment information, achieving a balance between robustness and economy without requiring exact distributions. However, moment-based methods only utilize the mean and covariance of the distribution, losing shape information such as multi-modality and skewness, which may still lead to conservative decisions.

A critical challenge lies in the fact that voltage and line flow constraints in distribution networks are inherently bilateral (with both upper and lower bounds). Most existing studies [5, 8] employ two separate one-sided chance constraints to approximate the upper and lower voltage limits, which essentially decomposes the joint bilateral constraint into two independent constraints, requiring two independent worst-case distributions for the upper and lower bounds, thereby introducing redundant conservativeness. Hou et al. [8] explicitly introduced the concept of joint two-sided chance constraints for soft open point (SOP) operation and exactly reformulated them into conic forms, avoiding the conservatism of one-sided approximation. However, their ambiguity set remained moment-based, and the potential of data-driven distribution estimation was not fully exploited.

From a data-driven perspective, kernel density estimation (KDE) offers a flexible nonparametric approach to capture the full shape of forecast error distributions directly from historical data, including multi-modality and skewness. Liu et al. [9] proposed a KDE-based distributionally robust mean-CVaR portfolio optimization model by combining weighted KDE with ϕ-divergence. By imposing weight constraints on KDE, they converted the infinite-dimensional space of probability density functions into a finite-dimensional convex optimization problem and proved convergence to the true distribution as the sample size increases. This methodology provides an important theoretical foundation for our work.

Inspired by the above research, this paper proposes a KDE-based distributionally robust chance-constrained optimization (KDE-DRCCO) model for the optimal load shedding problem in active distribution networks. The main contributions are as follows:

- A deterministic optimal load shedding model considering DG curtailment and load shedding is established using the linearized Distflow model [10], establishing a linear dependency between

decision variables and uncertainties;

- Voltage and line flow constraints perturbed by randomness are rigorously transformed into bilateral chance constraints, and a distributionally robust chance-constrained optimization model is formulated. Conditional value-at-risk (CVaR) approximation is employed to convert the probabilistic constraints into a computable form. Unlike existing approaches that use two separate one-sided constraints, our method directly handles joint bilateral constraints, avoiding redundant conservativeness;
- A data-driven kernel density estimation method is adopted to construct the error distribution, and a modified χ^2-divergence-based ambiguity set is formulated. The infinite-dimensional distributionally robust optimization problem is transformed into a finite-dimensional convex optimization problem via duality theory, and a rigorous convexity proof is provided. Compared with traditional moment-based methods, the KDE approach captures distribution shapes more accurately, reducing conservatism and operating costs while maintaining reliability;
- Simulations on modified IEEE 33-bus and IEEE 123-bus systems validate the economy and robustness of the proposed model, and the impacts of ambiguity set radius and risk parameters on model performance are analyzed.

The remainder of this paper is organized as follows. Section 2 introduces the linearized Distflow model and formulates the deterministic optimal load shedding problem. Section 3 presents the KDE-DRCCO model, where uncertainty modeling, KDE-based ambiguity set construction, CVaR approximation, and duality-based convex reformulation are discussed in detail. Section 4 describes the cutting plane algorithm and presents numerical results, including single-period and 24-hour dispatch analyses, sensitivity analysis, and non-Gaussian distribution validation on modified IEEE 33-bus and modified IEEE 123-bus systems. Section 5 concludes the paper.

2 Deterministic optimal load shedding model

2.1 Linearized distribution network power flow model

The power flow model is fundamental to the operation, planning, and optimization of power systems. From the perspective of grid structure, distribution networks typically exhibit a radial topology with branches characterized by high resistance-to-reactance ratios (r/x ratios), making the Branch Flow Model (BFM) more physically consistent with their characteristics than the bus injection model. The exact nonlinear BFM is formulated as follows[11]:

$$s_j = \sum_{i:i\to j} (S_{ij} - z_{ij}|I_{ij}|^2) - \sum_{k:j\to k} S_{jk}, \quad \forall j \in \mathcal{I} \setminus \{0\}, \tag{1}$$

$$S_{ij} = V_i I_{ij}^*, \quad \forall (i,j) \in \mathcal{B}, \tag{2}$$

$$V_j - V_i = z_{ij} I_{ij}, \quad \forall (i,j) \in \mathcal{B}. \tag{3}$$

In this model, V_i denotes a complex variable representing the voltage phasor that encompasses both magnitude and phase angle information; thereafter, it represents only the voltage magnitude. We first state the deterministic reformulation that underpins the proposed model.

Although the BFM is exact for all network structures, it exhibits a high degree of nonlinearity. In radial distribution networks, the Distflow model[11], which is derived by relaxing the phase

angle, is typically adopted:

$$p_j = (P_{ij} - r_{ij}\ell_{ij}) - \sum_{k:j\to k} P_{jk} \tag{4}$$

$$q_j = (Q_{ij} - x_{ij}\ell_{ij}) - \sum_{k:j\to k} Q_{jk} \tag{5}$$

$$v_j = v_i - 2(r_{ij}P_{ij} + x_{ij}Q_{ij}) + (r_{ij}^2 + x_{ij}^2)\ell_{ij} \tag{6}$$

$$\ell_{ij} = \frac{P_{ij}^2 + Q_{ij}^2}{v_i} \tag{7}$$

where $v_i = V_i^2$.

Proposition 1. *(Exactness of Distflow) [11]. In radial networks, the phase angle recovery condition is automatically satisfied; therefore, the Distflow model is exact.*

After introducing random variables, the nonlinear Distflow model struggles to characterize the impact of uncertainties in uncertainty analysis. Therefore, this paper adopts the LinDistflow model, which has a higher degree of linearization, to describe the power flow relationships in distribution networks, establishing a linear dependency between decision variables and uncertainties.

By neglecting the second-order high-order terms (network losses) and adopting the voltage assumption $(V_j - V_0)^2 \approx 0$, i.e., $V_j^2 \approx V_0^2 + 2V_0(V_j - V_0)$. The power balance equations are recursively solved along downstream nodes, while the voltage drop equations are recursively solved along upstream nodes. This yields the complete LinDistflow model [10]:

$$P_{ij} = \sum_{k\in\mathcal{W}(j)} p_k, \quad \forall (i,j) \in \mathcal{B}, \tag{8}$$

$$Q_{ij} = \sum_{k\in\mathcal{W}(j)} q_k, \quad \forall (i,j) \in \mathcal{B}, \tag{9}$$

$$V_i = V_0 - \sum_{j\in\mathcal{I}\setminus\{0\}} (p_j R_{ij} + q_j X_{ij}), \quad \forall i \in \mathcal{I}\setminus\{0\}, \tag{10}$$

where $\mathcal{W}(j)$ is the set of node j and its downstream nodes, and R_{ij}, X_{ij} are the sums of resistances and reactances, respectively, on the common path from the root node to nodes i and j.

Remark 1. *(Linearization accuracy) [10] Simulation results from the relevant literature show that the average relative error in voltage distribution between the exact power flow equations and the linearized power flow equations is 0.24%.*

Since the apparent power constraint $P_{ij}^2 + Q_{ij}^2 \le (S_{ij}^{\max})^2$ is nonlinear, this paper employs twelve convex polynomials to linearly approximate it. Let $\mathcal{S} = \{1, 2, \ldots, 12\}$. The linearized line capacity constraint is then expressed as [10]:

$$a_s P_{ij} + b_s Q_{ij} + c_s S_{ij}^{\max} \le 0, \quad \forall s \in \mathcal{S}. \tag{11}$$

2.2 Deterministic optimal load shedding model

In an active distribution network with photovoltaic (PV) generation and wind power installations, there exists a spatial-temporal mismatch between distributed generation and concentrated load demand. Typical scenarios include:

- Scenario 1: During midday, PV generation peaks while load demand is low. The network cannot absorb the surplus distributed generation, resulting in reverse power flow to the main grid and causing voltage rise violations. Consequently, a portion of the distributed generation injection needs to be curtailed.
- Scenario 2: During evening, PV generation drops while load demand peaks. The distributed generation cannot meet the load demand, causing undervoltage violations at the line terminals, necessitating load shedding.

Considering multi-period static optimization, the objective function is formulated to minimize the total operating cost, including the cost of power exchange with the main grid and the load shedding penalty [8]:

$$\min \sum_{t\in\mathcal{T}} \left(\eta_1 p_t^+ - \eta_2 p_t^- + \eta_3 \sum_{i\in\mathcal{I}\setminus\{0\}} p_{i,t}^{\text{cut}} \right) \Delta t, \tag{12}$$

where p_t^+ p_t^- are the power purchased from and sold to the main grid, respectively; $p_{i,t}^{\text{cut}}$is the amount of load shedding; η_1, η_2, η_3 are the corresponding price coefficients, with the penalty coefficient satisfying $\eta_3 \gg \eta_1 > \eta_2$.

The system power balance constraint is expressed as:

$$p_t^+ - p_t^- = \sum_{i\in\mathcal{I}\setminus\{0\}} p_{i,t}, \quad p_t^+ \geq 0, p_t^- \geq 0, \quad \forall t \in \mathcal{T}. \tag{13}$$

The net power demand constraint at node i is expressed as:

$$p_{i,t} = p_{i,t}^{\text{L}} - p_{i,t}^{\text{cut}} - p_{i,t}^{\text{DG}}(1-\lambda_{i,t}), \quad \forall i \in \mathcal{I}_{\text{DG}}, t \in \mathcal{T} \tag{14}$$

$$p_{i,t} = p_{i,t}^{\text{L}} - p_{i,t}^{\text{cut}}, \quad \forall i \in \mathcal{I} \setminus (\mathcal{I}_{\text{DG}} \cup \{0\}), t \in \mathcal{T} \tag{15}$$

$$q_{i,t} = q_{i,t}^{\text{L}} - q_{i,t}^{\text{cut}}, \quad \forall i \in \mathcal{I} \setminus \{0\}, t \in \mathcal{T} \tag{16}$$

where $\lambda_{i,t}$ is the curtailment ratio of distributed energy resources.

Meanwhile, the operational constraints on voltage and power, as well as the upper and lower bounds on the curtailment amount, are satisfied as follows:

$$V_{\min} \leq V_{i,t} \leq V_{\max}, \quad \forall i \in \mathcal{I} \setminus \{0\}, t \in \mathcal{T} \tag{17}$$

$$a_s P_{ij,t} + b_s Q_{ij,t} + c_s S_{ij}^{\max} \leq 0, \quad \forall (i,j) \in \mathcal{B}, t \in \mathcal{T}, s \in \mathcal{S} \tag{18}$$

$$0 \leq \lambda_{i,t} \leq 1, \quad \forall i \in \mathcal{I}_{\text{DG}}, t \in \mathcal{T} \tag{19}$$

$$0 \leq p_{i,t}^{\text{cut}} \leq p_{i,t}^{\text{L}}, \quad 0 \leq q_{i,t}^{\text{cut}} \leq q_{i,t}^{\text{L}}, \quad \forall i \in \mathcal{I} \setminus \{0\}, t \in \mathcal{T} \tag{20}$$

The LinDistflow power flow constraints are expressed as:

$$P_{ij,t} = \sum_{k\in W(j)} p_{k,t}, \quad \forall (i,j) \in \mathcal{B}, t \in \mathcal{T} \tag{21}$$

$$Q_{ij,t} = \sum_{k\in W(j)} q_{k,t}, \quad \forall (i,j) \in \mathcal{B}, t \in \mathcal{T} \tag{22}$$

$$V_{i,t} = V_0 - \sum_{j\in\mathcal{I}\setminus\{0\}} (p_{j,t} R_{ij} + q_{j,t} X_{ij}), \quad \forall i \in \mathcal{I} \setminus \{0\}, t \in \mathcal{T} \tag{23}$$

Theorem 1 (Convexity of the Deterministic Model)**.** *The deterministic optimal load shedding model* (12)-(23) *is a linear programming problem and therefore a convex optimization problem.*

3 KDE-DRCCO Model

3.1 Uncertainty Modeling

The uncertainties in active distribution networks mainly originate from forecast errors of loads and distributed energy resources. Let the load forecast error at node i in time period t be $\tilde{p}^{\mathrm{L}}_{i,t}$ and the DG forecast error be $\tilde{p}^{\mathrm{DG}}_{i,t}$. Then the random perturbation vector of the system can be defined as:

$$\xi_t = [\tilde{p}^{\mathrm{L}}_{1,t}, \ldots, \tilde{p}^{\mathrm{L}}_{n,t}, \tilde{p}^{\mathrm{DG}}_{1,t}, \ldots, \tilde{p}^{\mathrm{DG}}_{l_{\mathrm{DG}},t}]^\top \in \mathbb{R}^N. \tag{24}$$

Due to the adoption of the linearized power flow model (21)-(23), the system states (node voltages and branch power flows) exhibit affine characteristics with respect to the random variables. They can be decomposed into the sum of a deterministic base value (denoted by an overline $\overline{\bullet}$) and a random perturbation value (denoted by a tilde $\widetilde{\bullet}$) [8]:

$$P_{ij,t}(\xi_t) = \overline{P}_{ij,t} + \widetilde{P}_{ij,t}(\xi_t) = \overline{P}_{ij,t} + \sum_{k \in \mathcal{W}(j)} \tilde{p}_{k,t}, \tag{25}$$

$$V_{i,t}(\xi_t) = \overline{V}_{i,t} + \widetilde{V}_{i,t}(\xi_t) = \overline{V}_{i,t} - \sum_{j \in \mathcal{I} \setminus \{0\}} (\tilde{p}_{j,t} R_{ij} + \tilde{q}_{j,t} X_{ij}), \tag{26}$$

The reactive power flow $Q_{ij,t}$ has a similar affine translation form, where $q_{\tilde{k},t} = \tilde{p}_{k,t} \tan\theta$, and θ is the power factor angle.

3.2 Distributionally Robust Chance Constraints

To ensure that the system can still satisfy the security operation limits under uncertainties, chance constraints are introduced. However, the true probability distribution $\mathbb{P}$ is difficult to obtain exactly. We assume that the true distribution belongs to an ambiguity set $\mathcal{D}_t$ containing all possible probability distributions, and establish distributionally robust chance constraints [8]:

$$\inf_{\mathbb{P} \in \mathcal{D}_t} \mathbb{P}\big(V_{\min} \le V_{i,t}(\xi_t) \le V_{\max}\big) \ge 1 - \epsilon, \quad \forall i \tag{27}$$

$$\inf_{\mathbb{P} \in \mathcal{D}_t} \mathbb{P}\big(- c_s S^{\max}_{ij} \le a_s P_{ij,t}(\xi_t) + b_s Q_{ij,t}(\xi_t) \le c_s S^{\max}_{ij}\big) \ge 1 - \epsilon, \quad \forall ij, s. \tag{28}$$

where $\epsilon \in (0,1)$ is the allowable violation probability. To facilitate derivation, we unify the above bilateral chance constraints (27) and (28) into the following abstract form [8]:

$$\inf_{\mathbb{P} \in \mathcal{D}_t} \mathbb{P}\big(|\alpha_t^\top(\mathbf{x})\xi_t + \beta_t(\mathbf{x})| \le \gamma\big) \ge 1 - \epsilon, \tag{29}$$

where $\mathbf{x}$ represents the system decision variables, and the parameters $\alpha(\mathbf{x}), \beta(\mathbf{x}), \gamma$ can be directly mapped from the coefficients of (26) and (25).

For the voltage constraint (27), the specific parameters are:

$$\beta^V_{i,t}(\mathbf{x}) = \bar{V}_{i,t} - \frac{V_{\max} + V_{\min}}{2}, \quad \gamma^V_{i,t} = \frac{V_{\max} - V_{\min}}{2}, \tag{30}$$

$$\alpha^V_{i,t}(\mathbf{x}) = [\phi^{V,\mathrm{L}}_{i,t}(\mathbf{x}), \phi^{V,\mathrm{DG}}_{i,t}(\mathbf{x})], \tag{31}$$

where $\phi^{V,\mathrm{L}}_{i,t}(\mathbf{x}) = [-R_{ij} - X_{ij}\tan\theta, \forall j \in \mathcal{I} \setminus \{0\}]^\top$, $\phi^{V,\mathrm{DG}}_{i,t}(\mathbf{x}) = [(1-\lambda_{j,t})R_{ij}, \forall j \in \mathcal{I}_{\mathrm{DG}}]^\top$.

For the line capacity constraint (28), the parameters are:

$$\beta^{\mathrm{BC}}_{ij,t,s}(\mathbf{x}) = a_s \bar{P}_{ij,t} + b_s \bar{Q}_{ij,t}, \quad \gamma^{\mathrm{BC}}_{ij,t,s} = c_s S^{\max}_{ij}, \tag{32}$$

$$\alpha^{\mathrm{BC}}_{ij,t,s}(\mathbf{x}) = [\phi^{\mathrm{BC,L}}_{ij,t,s}(x), \phi^{\mathrm{BC,DG}}_{ij,t,s}(x)], \tag{33}$$

where

$$\phi^{\mathrm{BC,L},(k)}_{ij,t,s}(\mathbf{x}) = \begin{cases} a_s + b_s \tan\theta, & k \in W(j) \\ 0, & \text{otherwise} \end{cases},$$

$$\phi^{\mathrm{BC,DG},(k)}_{ij,t,s}(\mathbf{x}) = \begin{cases} -a_s(1-\lambda_{k,t}), & k \in W(j) \cap \mathcal{I}_{\mathrm{DG}} \\ 0, & \text{otherwise} \end{cases}.$$

3.3 Construction of Ambiguity Set Based on Kernel Density Estimation

To accurately characterize the distribution characteristics of forecast errors, weighted kernel density estimation is employed to perform nonparametric estimation of the random variable $g(\mathbf{x}, \xi) = \alpha^\top(\mathbf{x})\xi + \beta(\mathbf{x})$.

Definition 1 (Weighted Kernel Density Estimation)**.** [12] Given M samples $\{\xi_1, \ldots, \xi_M\}$, the transformed samples $\{g(\mathbf{x}, \xi_1), \ldots, g(\mathbf{x}, \xi_M)\}$ are obtained. The weighted KDE estimator is:

$$\hat{p}_\lambda(y) = \frac{1}{h} \sum_{m=1}^{M} \lambda_m k\left(\frac{y - g(\mathbf{x}, \xi_m)}{h}\right), \tag{34}$$

where $k(\cdot)$ is the Gaussian kernel function $k(u) = \frac{1}{\sqrt{2\pi}} e^{-u^2/2}$, which satisfies $k(t) \geq 0$, $\int k(t)dt = 1$, and $k(t) = k(-t)$. h is the bandwidth, and $\lambda = [\lambda_1, \ldots, \lambda_M]^\top$ is the sample weight vector.

Remark 2 (Bandwidth Selection)**.** *[13] This paper adopts the rule-of-thumb method for bandwidth selection: $h = 1.06\hat{\sigma}M^{-1/5}$, where $\hat{\sigma}$ is the sample standard deviation.*

The distribution uncertainty is transformed into the uncertainty of the weight vector λ, and the ambiguity set is constructed based on the ϕ-divergence.

Definition 2 (ϕ-Divergence Ambiguity Set)**.** [14] The ϕ-divergence-based ambiguity set is defined as:

$$\Lambda^\tau_\phi = \left\{ \lambda \in \mathbb{R}^M_+ \;\middle|\; \sum_{m=1}^{M} \lambda_m = 1, \frac{1}{M} \sum_{m=1}^{M} \phi(\lambda_m M) \leq \tau \right\}, \tag{35}$$

where $\phi(\cdot)$ is the divergence function, and τ is the radius of the ambiguity set, which controls the degree of distributional uncertainty.

Then the KDE-ϕ-divergence ambiguity set is:

$$\mathcal{P}^\tau_{KDE} := \left\{ \hat{p}_\lambda(y) = \frac{1}{h} \sum_{m=1}^{M} \lambda_m k\left(\frac{y - g(\mathbf{x}, \xi_m)}{h}\right), \lambda \in \Lambda^\tau_\phi \right\} \tag{36}$$

Lemma 1 (Conjugate Function of the Modified χ^2 Divergence)**.** *[15] For the modified χ^2 distance, i.e., $\phi(t) = (t-1)^2$ $(t \geq 0)$, its conjugate function is:*

$$\phi^*(s) = \begin{cases} s + s^2/4, & s \geq -2 \\ -1, & \textit{otherwise} \end{cases}. \tag{37}$$

3.4 CVaR Approximation and Convex Reformulation of Chance Constraints

Directly handling constraints containing probability operators (29) is a highly challenging non-convex NP-hard problem. This paper employs conditional value-at-risk (CVaR) to approximate them [16]:

$$\sup_{\mathbb{P}\in\mathcal{P}^{\tau}_{KDE}} \mathrm{CVaR}_{\epsilon}(|g(\mathbf{x},\xi)|-\gamma)\le 0 \iff \exists\eta\in\mathbb{R},\quad \eta+\frac{1}{\epsilon}\sup_{\mathbb{P}\in\mathcal{P}^{\tau}_{KDE}}\mathbb{E}_{\mathbb{P}}\left[[|g(\mathbf{x},\xi)|-\gamma-\eta]^{+}\right]\le 0. \quad (38)$$

where $[x]^{+}=\max(x,0)$, η is an auxiliary variable and is treated as a constant during the expectation evaluation.Let the auxiliary constant be $C=\eta+\gamma$. Substituting the weighted KDE estimator (34) into the expectation calculation, the expectation term can be analytically expanded using the integral properties of the kernel function.

Lemma 2 (KDE Representation of the Expectation Term)**.** *Based on the weighted KDE estimator* (34)*, the expectation term* $\mathbb{E}_{\mathbb{P}}[(|g(\mathbf{x},\xi)|-C)^{+}]$ *can be expressed as:*

$$\mathbb{E}_{\mathbb{P}}[[|g(\mathbf{x},\xi)|-C]^{+}]=\sum_{m=1}^{M}\lambda_m[\Psi(u_{1m})+\Psi(u_{2m})+C^{-}], \quad (39)$$

where $C^{+}=\max\{C,0\}$, $C^{-}=\max\{-C,0\}$, $u_{1m}=-g(x,\xi_m)-C^{+}$, $u_{2m}=g(x,\xi_m)-C^{+}$, *and*

$$\Psi(u)=h\left[u/hG(u/h)-\tilde{G}(u/h)\right],\quad G(u)=\int_{-\infty}^{u}k(t)dt,\quad \tilde{G}(u)=\int_{-\infty}^{u}tk(t)dt. \quad (40)$$

Proof. The proof proceeds by considering two cases based on the sign of C. For $C\ge 0$:

$$\begin{aligned}
\mathbb{E}_{\mathbb{P}}[[|g|-C]^{+}] &= \int_{-\infty}^{\infty}[|y|-C]^{+}\frac{1}{h}\sum_{m=1}^{M}\lambda_m k\left(\frac{y-g_m}{h}\right)dy\\
&= \frac{1}{h}\sum_{m=1}^{M}\lambda_m\left[\int_{-\infty}^{-C}(-y-C)k\left(\frac{y-g_m}{h}\right)dy+\int_{C}^{\infty}(y-C)k\left(\frac{y-g_m}{h}\right)dy\right]\\
&= \sum_{m=1}^{M}\lambda_m h\left[\int_{-\infty}^{(-g_m-C)/h}(-t+\frac{-g_m-C}{h})k(t)dt+\int_{-\infty}^{(g_m-C)/h}(-t+\frac{g_m-C}{h})k(t)dt\right]\\
&= \sum_{m=1}^{M}\lambda_m[\Psi(-g_m-C)+\Psi(g_m-C)].
\end{aligned}$$

For $C<0$:

$$\begin{aligned}
\mathbb{E}_{\mathbb{P}}[[|g|-C]^{+}] &= \mathbb{E}_{\mathbb{P}}[|g|-C]=\mathbb{E}_{\mathbb{P}}[|g|]-C\\
&= \sum_{m=1}^{M}\lambda_m[\Psi(-g_m)+\Psi(g_m)]-C.
\end{aligned}$$

By incorporating C^{+} and C^{-}, we can consolidate both cases into the unified expression given in (39). □

Although the analytical expression above appears intricate, it preserves the convexity of the original problem, which we formalize in the following proposition:

Proposition 2 (Joint Convexity)**.** *Let the reconstructed function be defined as* $F(y,C) = \Psi(-y - C^+) + \Psi(y - C^+) + C^-$*. Suppose* y *and* C *are affine functions of the decision variables. Then,* $F(y,C)$ *is everywhere continuously differentiable and jointly convex in* (y,C)*.*

Proof. To apply Theorem 5.5 of [17], we first express $F(y,C)$ as a piecewise-defined function:

$$F(y,C) = \begin{cases} \Psi(-y) + \Psi(y) - C, & C < 0, \\ \Psi(-y) + \Psi(y), & C = 0, \\ \Psi(-y - C) + \Psi(y - C), & C > 0. \end{cases}$$

It is straightforward to verify that $F(y,C)$ is continuous. We define the domain partitions $A_1 = \{(y,C)|C \le 0\}$ and $A_2 = \{(y,C)|C \ge 0\}$, both of which are closed convex sets. Define

$$\begin{aligned} f_1(y,C) =& \Psi(-y) + \Psi(y) - C + \iota_{A_1}(y,C), \\ f_2(y,C) =& \Psi(-y - C) + \Psi(y - C) + \iota_{A_2}(y,C), \end{aligned}$$

where $\iota_{A_i}(y,C) = \begin{cases} 0, & (y,C) \in A_i, \\ +\infty, & \text{otherwise.} \end{cases}$ Consequently, f_1 and f_2 are proper functions, and F can be represented as the lower envelope $F(y,C) = \min\{f_1(y,C), f_2(y,C)\}$.

We now prove that f_i are convex functions:

Case 1: $C < 0$. Then $F(y,C) = f_1(y,C) = \Psi(-y) + \Psi(y) - C$, and its Hessian matrix is:

$$\nabla^2 F(y,C) = \begin{pmatrix} \frac{1}{h}\left[k\left(-\frac{y}{h}\right) + k\left(\frac{y}{h}\right)\right] & 0 \\ 0 & 0 \end{pmatrix} \succeq 0, \tag{41}$$

Since $k(\cdot) > 0$, the Hessian is positive semidefinite, and f_1 is a proper convex function.

Case 2: $C > 0$. Then $F(y,C) = f_2(y,C) = \Psi(-y - C) + \Psi(y - C)$, and its Hessian matrix is:

$$\nabla^2 F(y,C) = \frac{1}{h}\begin{pmatrix} k\left(\frac{-y-C}{h}\right) + k\left(\frac{y-C}{h}\right) & k\left(\frac{-y-C}{h}\right) - k\left(\frac{y-C}{h}\right) \\ k\left(\frac{-y-C}{h}\right) - k\left(\frac{y-C}{h}\right) & k\left(\frac{-y-C}{h}\right) + k\left(\frac{y-C}{h}\right) \end{pmatrix}. \tag{42}$$

The determinant of the Hessian is given by:

$$\det \nabla^2 F = \frac{1}{h^2}\left[(k_- + k_+)^2 - (k_- - k_+)^2\right] = \frac{4}{h^2} k_- k_+,$$

where $k_- = k\left(\frac{-y-C}{h}\right)$, $k_+ = k\left(\frac{y-C}{h}\right)$. Since $k(\cdot) > 0$, we have $\det \nabla^2 F \ge 0$.Furthermore, the trace of the Hessian is strictly positive. Therefore, the Hessian matrix is positive semidefinite, implying that f_2 is a proper convex function on the interior of A_2.

At the boundary $C = 0$, we evaluate the directional limits of the gradients from the interiors of both subdomains:

$$\lim_{C \to 0^+} \frac{\partial F}{\partial C} = -G\left(-\frac{y}{h}\right) - G\left(\frac{y}{h}\right) = -1 = \lim_{C \to 0^-} \frac{\partial F}{\partial C}, \tag{43}$$

$$\lim_{C \to 0^+} \frac{\partial F}{\partial y} = -G\left(-\frac{y}{h}\right) + G\left(\frac{y}{h}\right) = \lim_{C \to 0^-} \frac{\partial F}{\partial y}, \tag{44}$$

which exist and are equal.

Since f_1 and f_2 are convex on their respective domains, the domains are compatible, and the gradient limits coincide at the boundary $C = 0$, all conditions of Theorem 5.5 in [17]are satisfied.Therefore, we conclude that $F(y,C)$ is globally convex and continuously differentiable on $\mathbb{R}^2$. □

Remark 3. *When $h \to 0$, $\Psi(u) = [u]^+$ [15].*

Substituting (39) into (38) and considering the worst-case distribution yields the distributionally robust optimization problem:

$$\exists \eta \in \mathbb{R}, \quad \text{s.t.} \quad \max_{\lambda \in \Lambda_\phi^\tau} \left\{ \eta + \frac{1}{\epsilon} \sum_{m=1}^{M} \lambda_m \left[\Psi(u_{1m}) + \Psi(u_{2m}) + C^- \right] \right\} \leq 0 \tag{45}$$

Theorem 2 (Duality Reformulation)**.** *The distributionally robust optimization problem* (45) *is equivalent to the following convex optimization problem:*

$$\exists \eta \in \mathbb{R}, \nu \geq 0, \mu \in \mathbb{R}, \quad s.t. \quad \eta + \nu\tau + \mu + \frac{\nu}{M} \sum_{m=1}^{M} \phi^* \left(\frac{d_m/\epsilon - \mu}{\nu} \right) \leq 0, \tag{46}$$

where $d_m = \Psi(u_{1m}) + \Psi(u_{2m}) + C^-$, and ϕ^* is the conjugate function of ϕ.

Proof. Construct the Lagrangian function:

$$\mathcal{L}(\lambda, \nu, \mu) = \eta + \frac{1}{\epsilon} \sum_{m=1}^{M} \lambda_m d_m + \nu \left(\tau - \frac{1}{M} \sum_{m=1}^{M} \phi(\lambda_m M) \right) + \mu \left(1 - \sum_{m=1}^{M} \lambda_m \right), \tag{47}$$

where $\nu \geq 0$, $\mu \in \mathbb{R}$ are dual variables, and the dual objective function is:

$$g(\mathbf{x}, \eta; \nu, \mu) = \max_{\lambda \geq 0} \mathcal{L}(\lambda, \nu, \mu)$$

Since $\lambda^0 = M^{-1}\mathbf{1} \in \Lambda_\phi^\tau$ satisfies $\mathbf{1}^\top \lambda^0 = 1$ and $\frac{1}{M} \sum_{m=1}^{M} \phi(\lambda_m^0 M) = 0 < \tau$, the interior of Λ_ϕ^τ is nonempty, and strong duality holds.

Taking the supremum with respect to the dual variable $\lambda \geq 0$:

$$\begin{aligned} g(\mathbf{x}, \eta; \nu, \mu) = \max_{\lambda \geq 0} \mathcal{L}(\lambda, \nu, \mu) &= \eta + \nu\tau + \mu + \max_{\lambda \geq 0} \sum_{m=1}^{M} \left[\frac{\lambda_m d_m}{\epsilon} - \lambda_m \mu - \frac{\nu}{M} \phi(\lambda_m M) \right] \\ &= \eta + \nu\tau + \mu + \frac{\nu}{M} \sum_{m=1}^{M} \max_{t_m \geq 0} \left\{ \frac{t_m}{\nu} \left(\frac{d_m}{\epsilon} - \mu \right) - \phi(t_m) \right\} \\ &= \eta + \nu\tau + \mu + \frac{\nu}{M} \sum_{m=1}^{M} \phi^* \left(\frac{d_m/\epsilon - \mu}{\nu} \right), \end{aligned}$$

where $t_m = \lambda_m M$. By strong duality, the original problem is equivalent to $\min_{\nu \geq 0, \mu} g(\mathbf{x}, \eta; \nu, \mu) \leq 0$. □

For the modified χ^2 distance, substituting the conjugate function and introducing auxiliary variables yields a computable form.

Corollary 1 (Computable Form for the Modified χ^2 Distance)**.** *[14] For the modified χ^2 distance, the distributionally robust constraint* (45) *is equivalent to:*

$$\eta + \mu + \nu(\tau - 1) + \frac{1}{4M\nu} \sum_{m=1}^{M} \left([v_m + 2\nu]^+ \right)^2 \leq 0, \tag{48}$$

$$\frac{1}{\epsilon} [\Psi(u_{1m}) + \Psi(u_{2m}) + C^-] - \mu \leq v_m, \quad \forall m, \tag{49}$$

where $v_m \in \mathbb{R}$ are auxiliary variables.

Proof. For the modified χ^2 distance, its conjugate function $\phi^*(s)$ can be uniformly expressed as:

$$\phi^*(s) = \frac{1}{4}([s+2]^+)^2 - 1$$

Substituting this expression into (46) and rearranging:

$$\eta + \nu\tau + \mu + \frac{\nu}{M}\sum_{m=1}^{M}\left(\frac{1}{4}\left(\left[\frac{d_m/\epsilon - \mu}{\nu} + 2\right]^+\right)^2 - 1\right) \leq 0$$

$$\eta + \nu\tau + \mu + \frac{1}{4M\nu}\sum_{m=1}^{M}\left([(d_m/\epsilon - \mu) + 2\nu]^+\right)^2 - \frac{\nu}{M}\sum_{m=1}^{M} 1 \leq 0$$

$$\eta + \mu + \nu(\tau - 1) + \frac{1}{4M\nu}\sum_{m=1}^{M}\left([(d_m/\epsilon - \mu) + 2\nu]^+\right)^2 \leq 0$$

Introduce auxiliary variables $v_m \in \mathbb{R}$. Replace $(d_m/\epsilon - \mu)$ with v_m, and relax $v_m = \frac{d_m}{\epsilon} - \mu$ to $\frac{d_m}{\epsilon} - \mu \leq v_m$, for computational tractability, yielding constraints (48)-(49). Since the left-hand side of inequality (48) is non-decreasing in v_m, replacing any v_m by a smaller value ,which still satisfying (49), does not worsen the inequality. Therefore, without loss of generality, we may set $v_m^* = \frac{d_m}{\epsilon} - \mu$, i.e., the relaxation is tight. □

3.5 Distributionally Robust Handling of the Objective Function

The electricity purchase and sale cost $\eta_1 p_t^+ - \eta_2 p_t^-$ in the objective function is also affected by randomness. From the power balance relationship:

$$p_t^+ - p_t^- = \sum_{i\in\mathcal{I}\setminus\{0\}} p_{i,t} = \sum_{i\in\mathcal{I}\setminus\{0\}} \tilde{p}_{i,t}^{\mathrm{L}} - \sum_{k\in\mathcal{I}_{\mathrm{DG}}} (1-\lambda_{k,t})\tilde{p}_{k,t}^{\mathrm{DG}} = \alpha_{\mathrm{obj},t}^{\top}(\mathbf{x})\xi_t, \tag{50}$$

we obtain $\alpha_{\mathrm{obj},t}(\mathbf{x}) = [\phi_{\mathrm{obj},t}^{\mathrm{L}}(\mathbf{x}), \phi_{\mathrm{obj},t}^{\mathrm{DG}}(\mathbf{x})]$, where $\phi_{\mathrm{obj},t}^{\mathrm{L}}(\mathbf{x}) = \mathbf{1}_{|\mathcal{I}|-1}$, $\phi_{\mathrm{obj},t}^{\mathrm{DG}(k)}(\mathbf{x}) = -(1-\lambda_{k,t})$.

Let $g_1(\mathbf{x},\xi) = \alpha_{\mathrm{obj},t}^{\top}(\mathbf{x})\xi$. Then the electricity purchase and sale cost can be expressed as:

$$\eta_1 p_t^+ - \eta_2 p_t^- = \frac{\eta_1 - \eta_2}{2}|g_1| + \frac{\eta_1 + \eta_2}{2} g_1. \tag{51}$$

Based on the KDE estimator, the expected value of (51) is:

$$\mathbb{E}_{\mathbb{P}}[\eta_1 p_t^+ - \eta_2 p_t^-] = \frac{\eta_1 - \eta_2}{2}\sum_{m=1}^{M}\lambda_m[\Psi(-g_{1m}, h) + \Psi(g_{1m}, h)] + \frac{\eta_1 + \eta_2}{2}\sum_{m=1}^{M}\lambda_m g_{1m}, \tag{52}$$

where $g_{1m} = \alpha_{\mathrm{obj},t}^{\top}(\mathbf{x})\xi_m$.

Using the same dual treatment as for the chance constraints, the worst-case expectation of the objective function is obtained:

$$\max_{\lambda\in\Lambda_\phi^\tau} \mathbb{E}_{\mathbb{P}}[\eta_1 p_t^+ - \eta_2 p_t^-] = \min_{\nu\geq 0,\mu}\left\{\nu\tau + \mu + \frac{\nu}{M}\sum_{m=1}^{M}\phi^*\left(\frac{1}{\nu}\left(\frac{\eta_1 - \eta_2}{2}[\Psi(-g_{1m}, h) + \Psi(g_{1m}, h)]\right.\right.\right.$$
$$\left.\left.\left. + \frac{\eta_1 + \eta_2}{2} g_{1m} - \mu\right)\right)\right\}. \tag{53}$$

3.6 Complete Formulation of the KDE-DRCCO Model

Integrating the above rigorous derivation from the non-convex model to CVaR and then to the dual equivalence, the final KDE-DRCCO model for active distribution networks can be formulated as the following convex programming model:

$$\min_{\mathbf{x},\nu,\mu,\eta,v} \quad \sum_{t\in\mathcal{T}}\Bigg(\eta_1\bar{p}_t^{+}-\eta_2\bar{p}_t^{-}+\eta_3\sum_{i\in\mathcal{I}\setminus\{0\}}p_{i,t}^{\mathrm{cut}}+\nu_{\mathrm{obj},t}(\tau-1)+\mu_{\mathrm{obj},t} + \frac{1}{4M\nu_{\mathrm{obj},t}}\sum_{m=1}^{M}\left([v_{\mathrm{obj},m,t}+2\nu_{\mathrm{obj},t}]^{+}\right)^2\Bigg)\Delta t \tag{54}$$

s.t. 1. Deterministic base-case LinDistflow equation constraints (21)-(23)

2. Node power balance and operational physical constraints (capacity limits, etc.)

3. Worst-case reconstruction boundary constraints for the main objective function:

$$\frac{\eta_1-\eta_2}{2}[\Psi(-g_{1m,t},h)+\Psi(g_{1m,t},h)]+\frac{\eta_1+\eta_2}{2}g_{1m,t}-\mu_{\mathrm{obj},t}\le v_{\mathrm{obj},m,t},$$
$$\forall m\in\{1,\dots,M\},\ \forall t\in\mathcal{T} \tag{55}$$

4. Distributionally robust chance constraints (for $\forall k\in\mathcal{K}$ covering all voltage and power chance constrai

$$\eta_{k,t}+\nu_{k,t}(\tau-1)+\mu_{k,t}+\frac{1}{4M\nu_{k,t}}\sum_{m=1}^{M}\left([v_{m,k,t}+2\nu_{k,t}]^{+}\right)^2\le 0, \tag{56}$$

$$\frac{1}{\epsilon}[\Psi(u_{1m,k,t},h)+\Psi(u_{2m,k,t},h)+C_{k,t}^{-}]-\mu_{k,t}\le v_{m,k,t}, \tag{57}$$

$$C_{k,t}=\gamma_k+\eta_{k,t},$$
$$u_{1m,k,t}=-g_{m,k,t}-C_{k,t}^{+},\quad u_{2m,k,t}=g_{m,k,t}-C_{k,t}^{+}, \tag{58}$$
$$g_{m,k,t}(\mathbf{x}_t,\xi_{m,t})=\alpha_k^{\top}(\mathbf{x}_t)\xi_{t,m}+\beta_k(\mathbf{x}_t). \tag{59}$$

All dual variables $\nu\ge 0$, μ,η,v involved are real numbers.

4 Numerical Experiments and Analysis

To verify the effectiveness and superiority of the proposed KDE-DRCCO model for optimal load shedding, numerical simulations are conducted on a modified IEEE 33-bus system (case33bw, detailed data in [18]) and a modified IEEE 123-bus system (grid_IEEE123, simplified to 114 nodes, detailed data in [19, 20]) active distribution networks.

To comprehensively evaluate the model performance, the following three optimization models are set up for comparison:

- **M1-Det**: Deterministic model that ignores uncertainties and solves the optimal power flow using only the forecast mean values.
- **M2-Moment**: Distributionally robust optimization model based on traditional first- and second-order moment information to construct the ambiguity set [8].
- **M3-KDE**: The proposed data-driven distributionally robust model based on kernel density estimation.

All numerical experiments are performed on a personal computer equipped with an 11th Gen Intel® Core™ i5-1135G7 @ 2.40 GHz CPU and 16 GB RAM. The M2 model is solved using YALMIP with the MOSEK solver, while the M1 and M3 models are solved using MATLAB's `fmincon` combined with the cutting plane method.

4.1 Cutting Plane Algorithm for KDE-DRCCO

Since the reformulated KDE-DRCCO model contains a large number of random scenarios incorporated through the nonlinear function Ψ, direct solution is extremely challenging. This paper adopts the Kelley cutting plane method based on outer approximation [21], decomposing the original problem into a master problem and subproblems that are solved alternately. The specific algorithm procedure is shown in Algorithm 1.

Algorithm 1 KDE-DRCC Cutting Plane Algorithm

Input: Network parameters $(\mathcal{N}, \mathcal{B}, r, x, V_{\min}, V_{\max}, S^{\max})$;
Uncertainty samples $\{\xi_1, \ldots, \xi_M\}$;
KDE parameter τ;
Tolerance $\epsilon_{feas} > 0$; maximum outer iterations $iter_{\max}$
Output: Optimal decision variables $x^* = [p^{cut}, q^{cut}, \lambda, p^+, p^-]$

Initialization:
Construct impedance matrices R, X
$\mathcal{C}_{cut} \leftarrow \emptyset$, $k \leftarrow 0$, set initial solution $x^{(0)}$
while $j < iter_{\max}$ **do**
  Solve the master problem:
  $x^{(j+1)} \leftarrow \arg\min_x f(x)$
    s.t. power balance, variable bounds, $\mathcal{C}_{cut}$
  Extract $\lambda^{(j+1)}$ and update $h^{(j+1)}$ based on the rule-of-thumb
  $Flag \leftarrow$ False
  for each chance constraint $k \in \mathcal{K}$ **do**
    Solve $F_k = \min_{\alpha,\eta,u} g_{dual}(\eta, \nu, \mu; x^{(j+1)}, h^{(j+1)})$
    if $F_k > \epsilon_{feas}$ **then**
      $Flag \leftarrow$ True
      $g_k \leftarrow \nabla_x F_k$
      $\mathcal{C}_{cut} \leftarrow \mathcal{C}_{cut} \cup \{g_k^T(x - x^{(j+1)}) + F_k \le 0\}$
    end if
  end for
  if $Flag =$ False **then**

    return $x^* \leftarrow x^{(j+1)}$
  end if
  $j \leftarrow j + 1$
end while

return x^*

4.2 Case Parameter Settings

The system rated voltage base value is 1 p.u., and the node voltage safety upper and lower limits are set to 1.05 p.u. and 0.95 p.u., respectively. Based on the MATPOWER default data, branches with zero limits are relaxed to twice the total base load of the system to ensure initial feasibility, and a regular dodecagon is used to linearly approximate the branch power flow constraints. The electricity purchase price η_1 and sales price η_2 are 0.09 \$/kWh and 0.045 \$/kWh, respectively, and the load shedding penalty coefficient η_3 is 0.3 \$/kWh. The load constant power factor is set to 0.85. The reliability requirement for the system's chance constraints is set to $\geq 95\%$ (i.e., violation risk tolerance $\epsilon = 0.05$).

In the 33-bus case system, four distributed generators (DGs) are connected at nodes 18, 22, 25, and 33, where nodes 18 and 25 are equipped with wind turbines (WT), and nodes 22 and 33 are equipped with photovoltaic (PV) systems. The rated capacity of each DG is uniformly 1.2 MW, and the total base active load of the system is 3.715 MW. In the 114-bus case system, five DGs are connected at nodes 30, 60, 80, 100, and 114. Among them, nodes 60 and 100 are equipped with WTs, and nodes 30, 80, and 114 are equipped with PV systems. The rated capacity of each DG is uniformly 1.65 MW, and the total base active load of the system is 3.490 MW.

To fully demonstrate the model characteristics, the experiments are divided into two parts: single-period scenario analysis and 24-hour optimal dispatch.

1) Single-period high-load scenario settings: Based on the 33-bus system and 114-bus system, the base load is scaled up by a factor of 1.3 to simulate a high-load scenario, and the single-unit forecast output is set to 10% of the local load at that node. The number of historical samples is $M = 100$, and the ϕ-divergence radius τ for KDE-DRCCO is set to 0.0001 (unless otherwise specified).

2) 24-hour multi-period scenario settings: The 33-bus and 114-bus systems are used for 24-hour dispatch testing. Load and DG outputs are generated according to typical diurnal fluctuation patterns, and the forecast curve schematic is shown in Fig. 1. The number of historical samples is $M = 100$, and the divergence radius τ is 0.0001 (unless otherwise specified).

The uncertainties mainly originate from forecast errors of loads and DG outputs. They are assumed to follow a Gaussian distribution with mean 0 and standard deviation equal to 15% of the forecast value. A total of 10,000 samples are generated to simulate historical data, from which a historical database is constructed by sampling. After optimization, an additional 5,000 Monte Carlo (MC) [22] samples are generated for reliability validation.

4.3 Single-Period Performance Comparison and Analysis

To intuitively analyze the underlying decision-making logic of the three models under the dual pressure of high load and uncertainty, a comparative analysis is first conducted in a single-period worst-case scenario (load scaled up by 1.3 times with insufficient distributed generation).

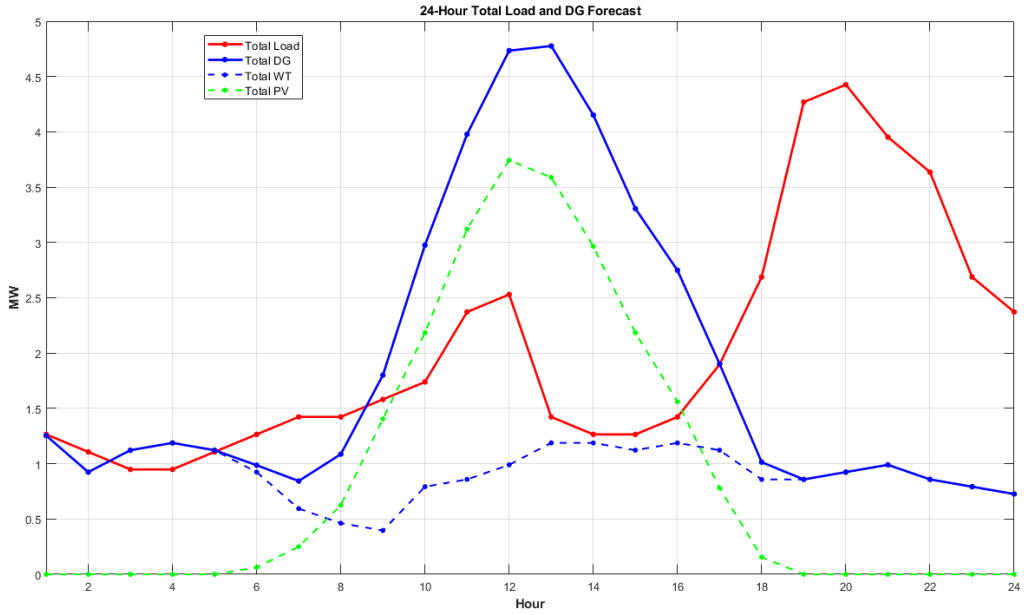

Figure 1: 24-hour load and DG forecast curves

Table 2: Performance comparison of three models in single-period high-load low-generation scenario (case33bw)

Evaluation Metric	**M1-Det**	**M2-Moment**	**M3-KDE**
Single-period cost ($\times 10^3$\$)	0.5451	0.6290	**0.5891**
Reliability (%)	34.20	100.00	97.00
Load shedding (MWh)	0.5629	0.9625	**0.7647**
MC voltage violation rate (%)	65.80	0.00	3.00

Table 3: Performance comparison of three models in single-period high-load low-generation scenario (grid_IEEE123)

Evaluation Metric	**M1-Det**	**M2-Moment**	**M3-KDE**
Single-period cost ($\times 10^3$\$)	0.4024	0.4677	**0.4191**
Reliability (%)	45.40	100.00	95.50
Load shedding (MWh)	0.0000	0.3108	**0.0736**
MC voltage lower bound violation rate (%)	54.60	0.00	4.50

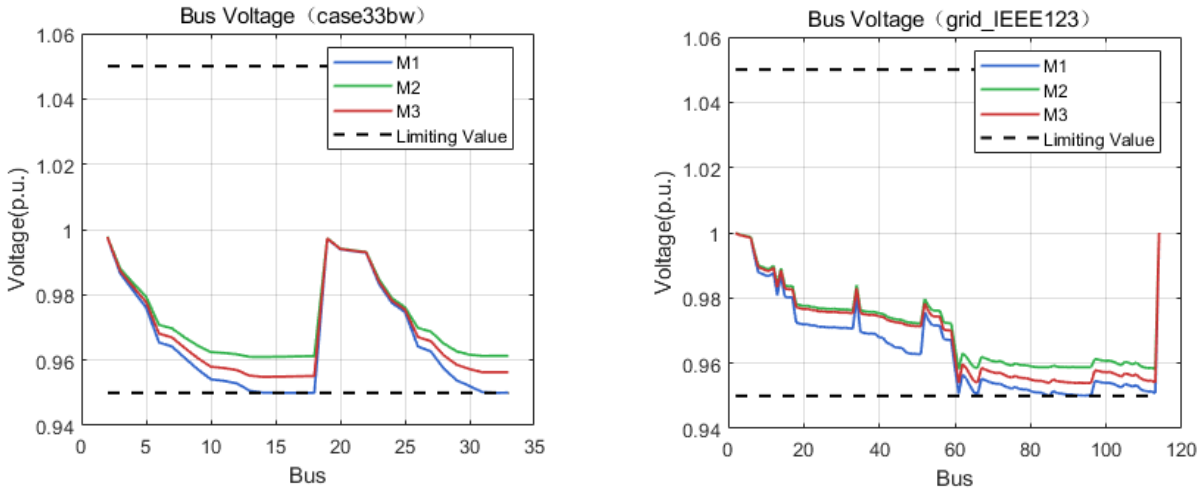

Figure 2: Comparison of node voltage distributions under the single-period worst-case scenario

Tables 2 and 3 together with Fig. 2 clearly reveal the essential differences among the models. In the high-load scenario with load scaled up by 1.3 times, the system's physical margin is extremely compressed. M1 completely ignores fluctuation errors and takes minimal load shedding measures, resulting in severe voltage drop risks of 65.8% and 54.6% in MC validation for the two cases, respectively. M2 perceives the risk and defends against it, but because the moment-based ambiguity set contains a large number of distributions, M2 is forced to shed 0.9625 MWh and 0.3108 MWh of load, respectively, leading to a sharp increase in cost.

In contrast, the proposed M3 model sheds only 0.7674 MWh and 0.0736 MWh of load, respectively, achieving high reliability of 97.0% and 95.5% (meeting the 95% requirement) while costing far less than M2. As shown in Fig. 2, the lower bound of the voltage distribution of M3 is closer to the 0.95 p.u. safety boundary, achieving a balance between economy and reliability.

4.4 24-Hour Multi-Period Optimal Dispatch Analysis

After clarifying the single-period characteristics, further validation is conducted on the case33bw and grid_IEEE123 systems under standard 24-hour dynamic dispatch scenarios. The results are shown in Tables 4 and 5, respectively.

Table 4: Comparison of 24-hour operation results (case33bw)

Evaluation Metric	**M1-Det**	**M2-Moment**	**M3-KDE**
24h total cost ($\times 10^3$\$)	1.0519	1.4194	**1.2954**
Actual reliability (%)	86.02	100.00	99.47
Total load shedding (MWh)	0.0286	1.2733	**0.4443**
Total DG curtailment (MWh)	0.1416	2.4992	**1.1429**

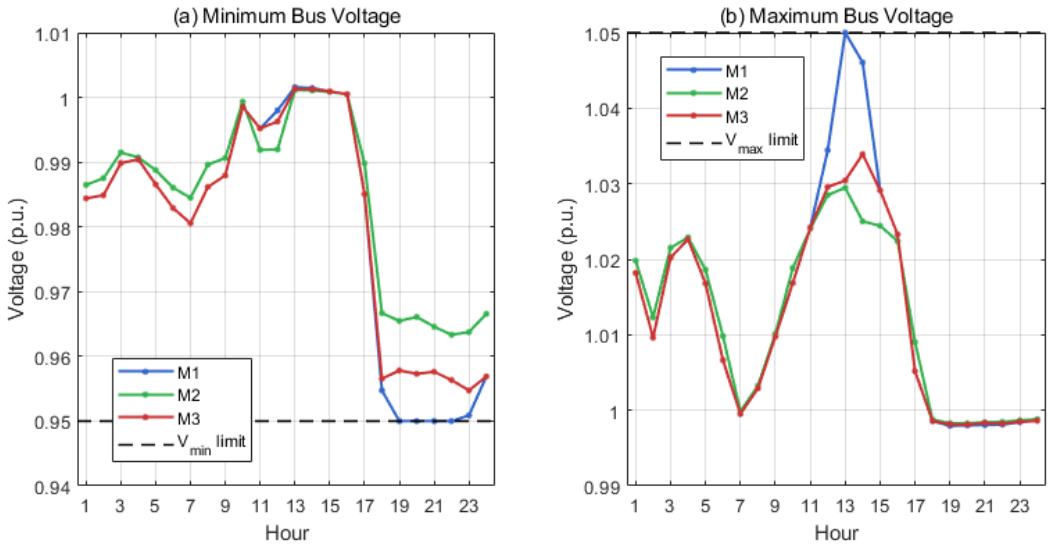

Figure 3: Comparison of 24-hour hourly minimum and maximum voltages for three models (case33bw)

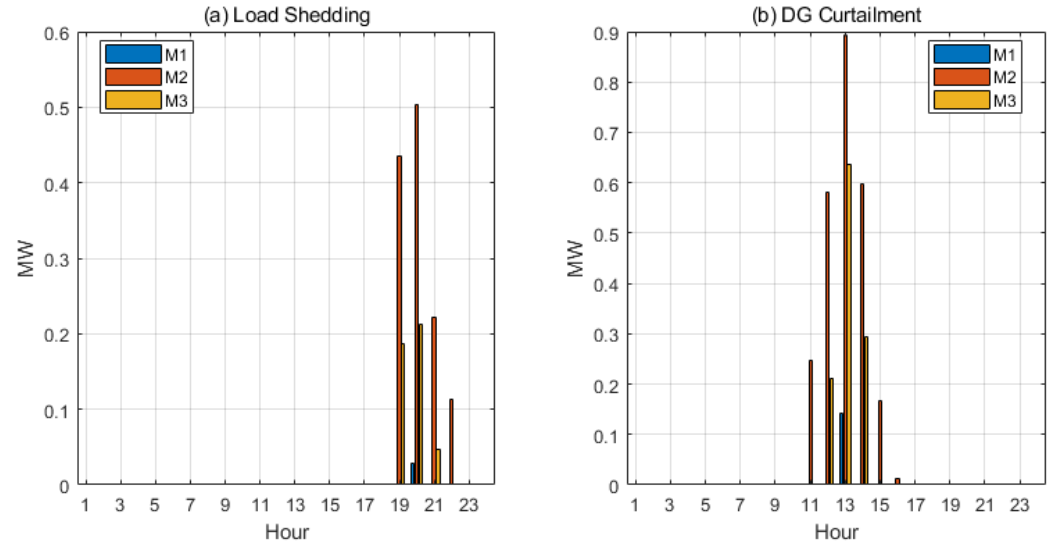

Figure 4: Comparison of 24-hour hourly active load shedding and DG curtailment for three models (case33bw)

Table 5: Comparison of 24-hour operation results (grid_IEEE123 large-scale system)

Evaluation Metric	**M1-Det**	**M2-Moment**	**M3-KDE**
24h total cost ($\times 10^3$\$)	0.5579	1.3911	**0.9802**
Actual reliability (%)	80.54	100.00	99.18
Total load shedding (MWh)	0.0261	3.5928	**1.1689**
Total DG curtailment (MWh)	0.0000	1.8710	**0.5869**

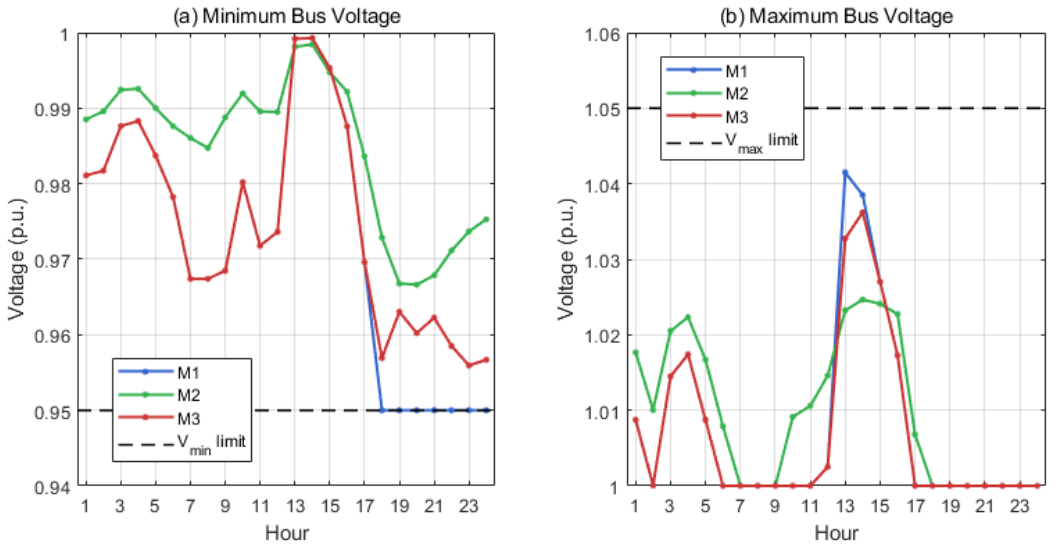

Figure 5: Comparison of 24-hour hourly minimum and maximum voltages for three models (grid_IEEE123)

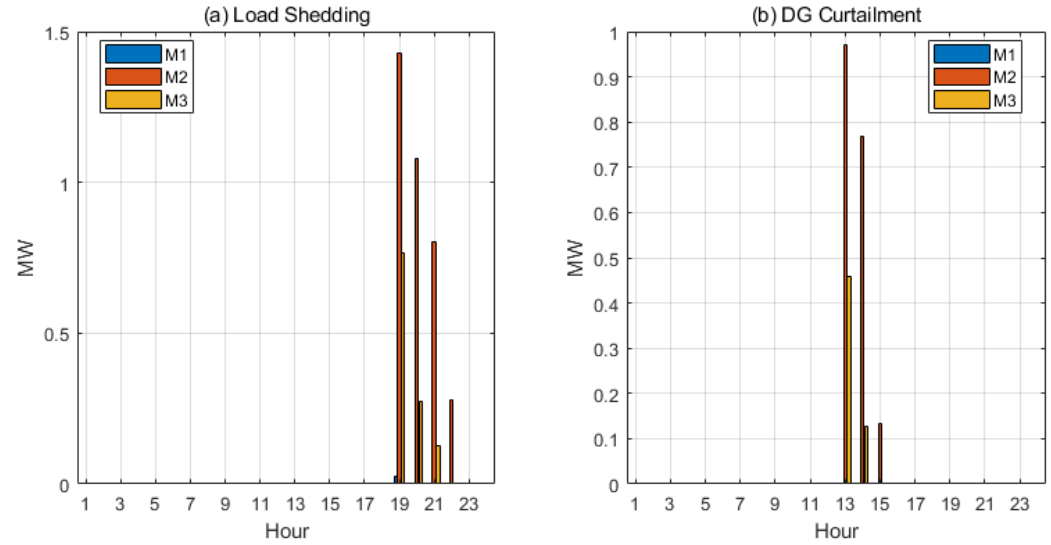

Figure 6: Comparison of 24-hour hourly active load shedding and DG curtailment for three models (grid_IEEE123)

As shown in Tables 4 and 5, the 24-hour dispatch results follow the same pattern as the single-period case. M2 is overly conservative, leading to excessive load shedding. In contrast, the proposed KDE-DRCCO model (M3), while strictly meeting the reliability requirement (both above 95%), significantly reduces load shedding and DG curtailment, thereby lowering the total cost. From Figs. 4 and 6, it can be seen that the KDE model, through data density learning, effectively suppresses the large amount of load shedding caused by the overly large moment-based ambiguity set during evening peak hours, achieving a balance between the security and economy of distribution network operation.

4.5 Sensitivity Analysis of the Ambiguity Set Radius τ

In the KDE-DRCCO model, the ϕ-divergence radius τ determines the range of the ambiguity set, reflecting the decision maker's trust in the data. This subsection conducts a sensitivity analysis of τ based on the 33-bus system to investigate its impact on cost and reliability.

Table 6: Results of τ parameter sensitivity analysis (case33bw)

τ	Total cost ($\times 10^3$\$)	Reliability (%)	Max violation (%)
0.00001	1.2922	99.40	2.94
0.00010	1.2954	99.41	2.90
0.00100	1.3055	99.45	2.62
0.01000	1.3364	99.57	1.82
0.05000	1.3531	99.58	1.82
0.10000	1.3523	99.50	2.24
0.50000	1.4839	99.67	1.52
1.00000	1.6003	99.77	1.12
M1-Det	1.0512	86.02	51.44
M2-Moment	1.4194	100.00	0.02

Table 6 shows that a larger τ leads to a more conservative model, with increasing cost but improving reliability. When τ is relaxed to a relatively conservative value of 0.1, the total cost of M3 (1352\$) is still lower than that of M2 (1419\$). However, when $\tau > 0.10$, the cost increases sharply, reaching 1600\$ at $\tau = 1.0$ (an 18.3% increase compared to $\tau = 0.05$), while the reliability improves by only 0.19%, indicating diminishing marginal returns.

4.6 Non-Gaussian Distribution Validation

In practical engineering, the forecast errors of wind and solar power outputs often exhibit certain non-Gaussian characteristics. To test the model's performance beyond Gaussian distributions, three non-Gaussian distributions—Logistic, Laplace, and Uniform—are used to generate test sets. To ensure fairness, the first and second moments of the samples generated from the three distributions are kept consistent with those of the original Gaussian distribution.

As shown in Table 7, the proposed KDE-DRCCO model (M3) maintains stable performance under all three different distributions: the total cost and reliability exhibit only minor variations. Compared with M2, M3 achieves a cost reduction of approximately 9.5%-10.6%, while maintaining comparable reliability. Compared with M1, M3 improves reliability by about 15%. These results validate the good performance of the proposed model under non-Gaussian distributions.

5 Conclusion

To address the supply-demand mismatch and operational risk violation problems in active distribution networks with high penetration of distributed energy resources, this paper innovatively extends the KDE method to the modeling and handling of bilateral chance constraints and applies it to the optimal load shedding problem in active distribution networks, proposing a data-driven distributionally robust chance-constrained optimal load shedding model based on KDE (KDE-DRCCO). This model not only achieves a reasonable description of uncertainties and a convex reformulation of bilateral chance constraints in theory but also makes significant breakthroughs in algorithms

Table 7: Performance validation under different non-Gaussian distribution scenarios

Distribution	Model	24h total cost ($\times 10^3$\$)		Reliability (%)	Voltage violation rate (%)	
		Optimized cost	MC cost		Average	Max
Logistic	M1-Det	1.0512	1.1273	86.15	13.85	51.52
	M2-Moment	1.4194	1.4890	99.98	0.02	0.16
	M3-KDE	**1.2694**	**1.2563**	99.42	0.91	4.58
Laplace	M1-Det	1.0519	1.1233	86.43	13.57	51.22
	M2-Moment	1.4194	1.4858	99.94	0.06	0.30
	M3-KDE	**1.2827**	**1.2648**	99.21	0.79	4.18
Uniform	M1-Det	1.0519	1.1309	86.01	13.99	50.72
	M2-Moment	1.4194	1.4900	100.00	0.00	0.00
	M3-KDE	**1.2803**	**1.2715**	99.64	0.36	2.82

and engineering applications. Specifically, this paper uses nonparametric KDE and ϕ-divergence to directly extract the probability density shape of forecast errors from historical data, overcoming the excessive conservatism of traditional moment-based ambiguity sets when handling bilateral chance constraints. While maintaining a confidence level above 95%, it effectively excludes interference from extremely adverse scenarios, significantly reducing operating costs and load shedding amounts. At the same time, by combining CVaR and strong duality theory, and utilizing the analytical integration properties of Gaussian kernel functions, the infinite-dimensional non-convex probability constraints introduced by KDE integration are rigorously and equivalently transformed into a finite-dimensional convex programming problem, laying a theoretical foundation for efficient solution of the model. The outer-approximation-based cutting plane algorithm can stably converge to the global optimal solution in multi-period optimal load shedding dispatch on the modified IEEE 123-bus system. Out-of-sample validation further shows that the model has good adaptability and robust security to non-normal forecast errors commonly encountered in practical engineering, effectively balancing the economy and security of distribution network operation.

References

[1] J. Liu, P. Zeng, H. Xing, Y. Li, Q. Wu, Optimal operation of flexible distribution networks for security improvement considering active management, CSEE Journal of Power and Energy Systems 9 (3) (2020) 996–1007.

[2] H. Ji, C. Wang, P. Li, F. Ding, J. Wu, Robust operation of soft open points in active distribution networks with high penetration of photovoltaic integration, IEEE Transactions on Sustainable Energy 10 (1) (2019) 280–289.

[3] V. Calderaro, V. Galdi, G. Graber, A. Piccolo, Generation rescheduling and load shedding in distribution systems under imprecise information, IEEE Systems Journal 12 (1) (2016) 383–391.

[4] Y. Zhang, S. Moura, Stochastic optimal load shedding with heterogeneous load zones, in: 2020 IEEE Power & Energy Society Innovative Smart Grid Technologies Conference (ISGT), IEEE, 2020, pp. 1–5.

[5] M. Rayati, M. Bozorg, R. Cherkaoui, M. Carpita, Distributionally robust chance constrained optimization for providing flexibility in an active distribution network, IEEE Transactions on Smart Grid 13 (4) (2022) 2920–2934.

[6] E. Delage, Y. Ye, Distributionally robust optimization under moment uncertainty with application to data-driven problems, Operations Research 58 (3) (2010) 595–612.

[7] W. Wiesemann, D. Kuhn, M. Sim, Distributionally robust convex optimization, Operations Research 62 (6) (2014) 1358–1376.

[8] Q. Hou, G. Chen, N. Dai, H. Zhang, Distributionally robust chance-constrained optimization for soft open points operation in active distribution networks, CSEE Journal of Power and Energy Systems (2022).

[9] W. Liu, L. Yang, B. Yu, Kernel density estimation based distributionally robust mean-cvar portfolio optimization, Journal of Global Optimization 84 (4) (2022) 1053–1077.

[10] S. Wang, S. Chen, L. Ge, L. Wu, Distributed generation hosting capacity evaluation for distribution systems considering the robust optimal operation of oltc and svc, IEEE Transactions on Sustainable Energy 7 (3) (2016) 1111–1123.

[11] M. Farivar, S. H. Low, Branch flow model: Relaxations and convexification—part i, IEEE Transactions on Power Systems 28 (3) (2013) 2554–2564.

[12] Q. Li, J. S. Racine, Nonparametric econometrics: theory and practice, Princeton University Press, 2007.

[13] M. C. Jones, J. S. Marron, S. J. Sheather, A brief survey of bandwidth selection for density estimation, Journal of the American statistical association 91 (433) (1996) 401–407.

[14] A. Ben-Tal, D. Den Hertog, A. De Waegenaere, B. Melenberg, G. Rennen, Robust solutions of optimization problems affected by uncertain probabilities, Management Science 59 (2) (2013) 341–357.

[15] R. T. Rockafellar, Convex analysis, Vol. 28, Princeton university press, 1997.

[16] R. T. Rockafellar, S. Uryasev, et al., Optimization of conditional value-at-risk, Journal of risk 2 (2000) 21–42.

[17] H. H. Bauschke, Y. Lucet, H. M. Phan, On the convexity of piecewise-defined functions, ESAIM: Control, Optimisation and Calculus of Variations 22 (3) (2016) 728–742.

[18] S. H. Dolatabadi, M. Ghorbanian, P. Siano, N. D. Hatziargyriou, An enhanced ieee 33 bus benchmark test system for distribution system studies, IEEE Transactions on Power Systems 36 (3) (2020) 2565–2572.

[19] L. Bobo, A. Venzke, S. Chatzivasileiadis, Second-order cone relaxations of the optimal power flow for active distribution grids, arXiv preprint arXiv:2001.00898 (2020).

[20] W. H. Kersting, Radial distribution test feeders, in: 2001 IEEE Power Engineering Society Winter Meeting. Conference Proceedings (Cat. No. 01CH37194), Vol. 2, IEEE, 2001, pp. 908–912.

[21] J. E. Kelley, Jr, The cutting-plane method for solving convex programs, Journal of the society for Industrial and Applied Mathematics 8 (4) (1960) 703–712.

[22] S. Shah, Monte carlo simulation in renewable energy planning: A comprehensive review and novel framework for uncertainty quantification, Emerging Frontiers Library for The American Journal of Engineering and Technology 7 (06) (2025) 24–45.